Redox and Ligand Exchange during the Reaction of Tetrachloroaurate with Hexacyanoferrate(II) at a Liquid-Liquid Interface: Voltammetry and X-ray Absorption Fine-Structure Studies

Akihiro Uehara[a,b,*], Sin-Yuen Chang[c,e], Samuel G. Booth[b], Sven L.M. Schroeder[d,e], J.Frederick W. Mosselmans[e], Robert A.W. Dryfe[b]

[a] Division of Nuclear Engineering Science, Research Reactor Institute, Kyoto University, Asashironishi, Kumatori, Osaka, 590-0494, Japan
[b] School of Chemistry, The University of Manchester, Oxford Road, Manchester, M13 9PL, United Kingdom
[c] School of Chemical Engineering and Analytical Science, The University of Manchester, Oxford Road, Manchester, M13 9PL, United Kingdom
[d] School of Chemical and Process Engineering, Faculty of Engineering, The University of Leeds, Leeds LS2 9JT, United Kingdom
[e] Diamond Light Source Ltd., Didcot, Oxfordshire, OX11 0DE, United Kingdom

ARTICLE INFO

ABSTRACT

Voltammetry for charge (ion and electron) transfer at two immiscible electrolyte solutions (VCTIES) has been used to provide insight into the ligand exchange and redox processes taking place during the interfacial reaction of aqueous hexacyanoferrate(II) with tetrachloroaurate ($[AuCl_4]^-$) in 1,2-dichloro-ethane (DCE). VCTIES permitted the detection of the reactants, intermediates and products at the liquid/liquid interface. A model for the sequence of interfacial processes was established with the support of speciation analysis of the key elementary reactions by X-ray absorption spectroscopy (XAS). The potential-driven transfer of $[AuCl_4]^-$ from the organic into the aqueous phase is followed by reduction and ligand exchange by the aqueous hexacyanoferrate(II) to form dicyanoaurate ($[Au(CN)_2]^-$). Inferences from the reactions point to the likely formation of $[AuCl_2]^-$ during the reduction sequence. The reaction is influenced by ligand exchange equilibria between $[AuCl_4]^-$, $[AuCl_3(OH)]^-$ and $[AuCl_2(OH)_2]^-$ which are shown to be dependent on the chloride ion concentration and pH of the solution. The difference between the Gibbs energy of transfer at the water | DCE interface ($\Delta_{DCE}^W G°$)of $AuCl_4^-$ and $[AuCl_3(OH)]^-$, and the difference between $[AuCl_3(OH)]^-$ and $[AuCl_2(OH)_2]^-$ were found to change by a value close to the difference between $\Delta_{DCE}^W G°$ of Cl^- and that of OH^-. The intermediate Au(I) species, $[AuCl_2]^-$, was seen to decompose at neutral pH and in the absence of Cl^- in water to form metallic Au, although it was stable in >10 mM HCl for an hour. Time-dependent VCTIES and X-ray absorption fine structure (XAFS) speciation analysis of the homogeneous aqueous phase indicate that reaction between $[AuCl_4]^-$ and hexacyano-ferrate(II) is accompanied by the formation of an intermediate ionic species, formed when the concentration of $[AuCl_4]^-$ is close to that of hexacyanoferrate(II). This species, whose identity was not precisely determined, was also generated by reaction between $[AuCl_2]^-$ and hexacyanoferrate(III). The species is shown by VCTIES to be more hydrophilic than $[Au(CN)_2]^-$, $[AuCl_2]^-$ and $[AuCl_4]^-$.

1. Introduction

Au(III) and Au(I) complexes in aqueous solution can undergo simultaneous transformations such as ligand substitution and redox reactions, which are of particular interest due to their importance in the synthesis of metallic Au nanoparticles, and the extraction/purification of the metal. The redox transformations between Au(III), Au(I) and Au(0) species are influenced by reducing agents, coexisting ligands, electrolytes, and pH, resulting in Au complexes with varying standard redox potentials in water [1–5].

The reaction between tetrachloroaurate, $[AuCl_4]^-$ and hexa-cyanoferrate(II) (ferrocyanide, $[Fe(CN)_6]^{4-}$) has previously been examined [6–10]. It was proposed that hexacyanoferrate(II), used as a reducing agent, produced dicyanoaurate, $[Au(CN)_2]^-$, as well as complexes of Fe^{3+} and $[AuCl_2]^-$ [6–8]. On the other hand, hexacyanoferrate(III) (ferricyanide, $[Fe(CN)_6]^{3-}$) was employed to decrease the size of Au nanoparticles previously prepared by the oxidation of Au(0) [6]. The pH and electrolyte dependence of

* Corresponding author. Tel.: +81 724 51 2454.
E-mail address: auehara@rri.kyoto-u.ac.jp (A. Uehara).

aqueous Au(III) and Au(I) species need to be taken into consideration when modelling the reduction process though the thermodynamic properties of species such as $[AuCl_3(OH)]^-$ and $[AuCl_2(OH)_2]^-$ [11,12]. Au(I) chloro-complexes, which are plausible reduction intermediates, also readily decompose by disproportionation to Au(III) and metallic Au [13]. Voltammetry for charge (ion and electron) transfer between two immiscible electrolyte solutions (VCTIES) has been used to investigate the reduction of Au ions where the Au species are initially located in an organic phase in contact but immiscible with the aqueous phase containing the reducing reagent. Au deposition at the liquid/liquid interface is well known having been the subject of a number of previous studies including [9,10,14–20]. In the case of hexacyanoferrate, the charge transfer current corresponding to the reduction of $[AuCl_4]^-$ and the concomitant oxidation of hexacyanoferrate(II) has been observed [9,10]. This reaction relies on the initial transfer of $[AuCl_4]^-$ from the organic to the aqueous phase which is then followed by a homogeneous reaction with hexacyanoferrate(II) to form Au(I), $[AuCl_2]^-$. VCTIES can be applied to identify the ionic species based on their ion transfer potential between the aqueous and organic solutions, which is proportional to the difference in solvation energy of ions between the two solutions [21]. The electrochemical transfers of $[AuCl_4]^-$ [9,10,14,17–20], $[AuBr_4]^-$ [10] or $[AuCl_2]^-$ [19,20] between water and organic solutions have been reported, however, the transfers of other Au complexes are, to the best of our knowledge, yet to be reported.

Our VCTIES have been combined with X-ray absorption fine structure (XAFS) measurements which can provide detailed information about the local structure around the atoms of a specific element. The coordination structure of Au complexes have been examined in detail, including the identification of valency from X-ray absorption near-edge structure (XANES)[20,22], and characterization of Au—Cl [23–26], Au—OH [23–25] and Au—CN [26,27] bonds through the analysis of extended X-ray absorption fine-structure (EXAFS). As XAFS is an elementally specific technique, in-situ XAFS measurements are capable of identifying Au(III), Au(I) and Au(0) species formed in the presence of reducing agents [25,26,28,29] or at high temperature [30]. As such, XAFS analysis of the homogenous solutions provides quantitative understanding of the ligand exchange reactions of the Au complexes and their redox reactions.

In the present study, we combine VCTIES measurements and XAFS as complimentary techniques to understand the interfacial reaction between Au ions and hexacyanoferrate(II). The ionic species $[AuCl_4]^-$ and $[AuCl_2]^-$ formed in aqueous solutions were found to be dependent on the concentrations of H^+, electrolyte and hexacyanoferrate(III) and (II) in the system. From these observations we discuss a possible mechanism for the redox process between hexacyanoferrate(II) in aqueous solution and $[AuCl_4]^-$ in organic solution.

2. Experimental

2.1. Chemicals

Hydrogen tetrachloroaurate, $HAuCl_4·3H_2O$ (≥99.99%, Alfa Aesar) was used as the source of Au(III). HCl, LiCl and Li_2SO_4 (≥99%, Aldrich) were used as electrolytes in the aqueous phases. 1,2-dichloroethane, DCE (≥99%, Aldrich) and 1,2-dichlorobenzene, DCB (≥99%, Aldrich) were used as the organic solvents. Tetraoctylammonium tetrachloroaurate, denoted as $TOA^+[AuCl_4]^-$, was obtained as a precipitate by mixing methanol solutions of TOA^+Cl^- (≥97%, Aldrich) and $H^+[AuCl_4]^-$, and was purified by recrystallization in ethanol [3]. $TOA^+[AuCl_2]^-$ in DCE was used as the source of Au(I) which was prepared by mixing water with DCE containing equimolar tetrabutylammonium dichloroaurate, $TBA^+[AuCl_2]^-$

(Tokyo Chemical Industry UK Ltd.) and TOA^+Cl^-. An aqueous solution of 5 mM $KAu(CN)_2$ (99.98%, Aldrich) was also measured as a reference XANES spectrum used for linear combination fitting. The stability of $[AuCl_2]^-$ in water was investigated using an aqueous solution of $[AuCl_2]^-$ prepared by exchange with $[AuCl_4]^-$ as described in the experimental section. Here, a DCE solution containing 5 mM $[AuCl_2]^-$ was mixed with water containing 0.1 M HCl and 4 mM $[AuCl_4]^-$. Through mixing 4 mM of $[AuCl_2]^-$ was extracted into the water phase, see Eq. (1). The process is an ion-exchange, driven by the greater hydrophilicity of the Au(I) halide over its Au(III) counterpart (Table 1). The batch system was employed because it is difficult to dissolve $[AuCl_2]^-$ as its TOA^+ salt into water.

$$[AuCl_4]^-_{(W)} + TOA^+[AuCl_2]^-_{(DCE)}$$
$$\rightleftharpoons TOA^+[AuCl_4]^-_{(DCE)} + [AuCl_2]^-_{(W)} \qquad (1)$$
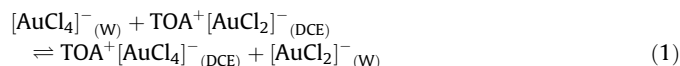
Here, W denotes the aqueous solution. The supporting electrolyte in DCE was $BTPPA^+TFPB^-$ and TOA^+TFPB^-, where $BTPPA^+$ and $TFPB^-$ denote the bis(triphenylphosphoranylidene) ammonium and tetrakis[3,5-bis(trifluoromethyl) phenyl]borate ions, respectively. $BTPPA^+TFPB^-$ and TOA^+TFPB^- were obtained as precipitates after mixing a methanol solution of $BTPPA^+Cl^-$ (≥97%, Alfa Aesar) or TOA^+Cl^- with a methanol solution of Na^+TFPB^- (≥97%, Alfa Aesar), the product was purified by recrystallization in ethanol.

2.2. Measurement of the voltammogram for charge transfer at the macro and micro water | DCE interface

Two electrochemical cells were employed for the VCTIES: one with a macroscale and one with a micro-scale contact between the two phases. In a conventional macro-interface cell [10], cyclic voltammetry experiments were performed using a four electrode configuration with an IVIUM "Compactstat" potentiostat (IVIUM Technologies, the Netherlands). No iR compensation was applied for the electrochemical measurements. Homemade Ag|AgCl and platinum gauze were used as the reference electrodes (RE) and counter electrodes (CE) respectively. The counter electrode in DCE was coated with glass to avoid the contact of platinum with water. The water | DCE interface had a cross-sectional area of $0.64\ cm^2$ and a volume of $2\ cm^3$. Further details are described elsewhere [10]. The micro-interface cell consists of a water chamber and a DCE chamber separated by a 16 μm thick polyester film with a micro hole 30 μm in diameter. The water | DCE interface was formed at the micro hole [31–33].

In both cells, the potential difference at the water | DCE interface, E, was measured. The potential of an Ag|AgCl electrode in water, was referred to the potential of a $BTPPA^+$ ion selective electrode inserted in DCE. The generic cell composition is:
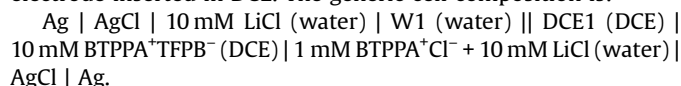
Ag | AgCl | 10 mM LiCl (water) | W1 (water) || DCE1 (DCE) | 10 mM $BTPPA^+TFPB^-$ (DCE) | 1 mM $BTPPA^+Cl^-$ + 10 mM LiCl (water) | AgCl | Ag.

Table 1
Standard ion transfer potential between water and DCE.

Ions	$\Delta_{DCE}^W \phi°$ (V vs. TPhE)	$\Delta_{DCE}^W G°$ (kJ mol^{-1})
$[AuCl_4]^-$ (**peak A**)	0.115 [19]	−11.1
$[AuCl_3(OH)]^-$ (**peak B**)	−0.064	6.2
$[AuCl_2(OH)_2]^-$ (**peak C**)	−0.254	24.5
$[AuCl_2]^-$ (**peak D**)	0.026 [19]	−2.5
$[Au(CN)_2]^-$ (**peak E**)	−0.036	3.5
Cl^-	−0.530 [37], −0.479 [39]	51.1, 46.2
OH^-	−0.701 [37], −0.656 [39]	67.6, 63.3

E is related to the Galvani potential difference, $\Delta_{DCE}^{W}\phi$, as

$$E = \Delta_{DCE}^{W}\phi + E_{ref} \tag{2}$$

Where E_{ref} is the potential of the reference electrodes employed. In the calculations of the Gibbs energy of ion transfer between water and DCE, $\Delta_{DCE}^{W}G^{\circ}(= -zF\Delta_{DCE}^{W}\phi^{\circ}, z$ and F are the charge and the Faraday constant), the measured *E* was converted using the extra-thermodynamic assumption of Parker [34].

2.3. XAFS measurements

XAFS spectra were acquired at the spectroscopy beamline I18 of DIAMOND Light Source (Harwell Science and Innovation Campus, UK) [35]. All measurements were collected in fluorescence-yield mode using an Ortec multi-element solid-state Ge detector to measure the Au L_3 edge. The electron storage ring runs at 3 GeV with a current of 300 mA. A double crystal Si(111) monochromator with an intrinsic resolution of 1.4×10^{-4} $\Delta E/E$ was used. When using the full beam the flux at the gold L_3-edge is 8×10^{11} photons. Each measurement took ~30 min. The beam size was ~420 μm × 280 μm. The strong XANES resonance visible in the spectra at about 11 918 eV reflects an intra-atomic electronic transition of Au $2p_{3/2}$ core electrons to unoccupied valence states. Spectral features in the Au L_3-edge XANES beyond this photon energy range are additionally influenced by back scattering of photoelectrons. The high sensitivity of XAFS to unoccupied valence 5d and 6s-states of Au allows the identification of the oxidation state, electronic configuration and coordination geometry.

For each measurement, a 1 mL sample solution was placed in a 1.5 mL Eppendorf microcentrifuge tube positioned vertically on a magnetic stirrer plate. XAFS analysis were carried out using the Demeter software package [36]. Energy scales were calibrated according to a standard procedure where the first inflection point of gold foil is known to be 11 919 eV. EXAFS for the Au—Cl—OH system (Table 2) were fitted in FT-space using simultaneous k_1, k_2 and k_3 weightings where k is the photoelectron wave vector. A Hanning-type window with dk = 1 was used for Fourier Transformation from k-space into FT-space. A k-range of 3–12 Å^{-1} and R-range of 1–4 Å were used for the fittings, except for the pH 11.77 sample where the window ranges are 3–10 Å^{-1} and 1.25–4 Å. One energy shift parameter (ΔE_0) was used for all of the shells. To account for the changes in relative Au(III) and Au(0) compositions, $x_{Au(III)}S_0^2$ and $x_{Au(0)}S_0^2$ were assigned to each fit where x denotes composition and S_0^2 denotes amplitude reduction factor. Note that $x_{Au(III)}S_0^2$ and $x_{Au(0)}S_0^2$ almost always sum to ~0.9. Any instances in the text referring to FT-peak before phase shift will be indicated.

Linear combination fitting for the Au—Cl—CN system (Fig. 8) was carried out over the range of 11 899 to 11 949 eV. The samples for the Au–Cl–CN system were measured as soon as possible after sample preparation; ~30 min gap between sample preparation and XAFS measurements.
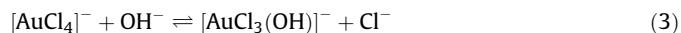
3. Results and discussion

The stability of [AuCl$_4$]$^-$ and [AuCl$_2$]$^-$ ions as a function of H$^+$ concentration and electrolytes (in the absence of hexacyanoferrate) was first studied (sections 3.1 and 3.2 respectively) with the aim to prevent decomposition of these Au species. Once the solution conditions that stabilize these gold chloride ions were found, the reactions between [AuCl$_4$]$^-$ or [AuCl$_2$]$^-$ with hexacyanoferrate (II) or (III) were investigated by VCTIES and XAS (sections 3.3 and 3.4).

3.1. Stability of [AuCl$_4$]$^-$ as a function of pH and Cl$^-$ concentration

The dependence of [AuCl$_4$]$^-$ stability on Cl$^-$ concentration and pH has been investigated previously by UV-visible spectroscopy [11]. VCTIES is introduced here as an alternative method to determine the stability of [AuCl$_4$]$^-$ in water at various pH and Cl$^-$ concentrations. The stability of [AuCl$_4$]$^-$ in an acidic aqueous solution was examined by cyclic voltammogram (CV) recorded at the interface between an aqueous phase containing Na$^+$[AuCl$_4$]$^-$ (0.2 mM) in 10 mM HCl (pH = 2) and DCE (10 mM TOA$^+$TFPB$^-$). Positive and negative current features at 0.148 and 0.082 V corresponding to the transfer of [AuCl$_4$]$^-$ between water and DCE were observed. The mid-point potential was calculated to be 0.115 V (**peak A**) which is close to the previously reported values [9,10].

When HCl was replaced by 10 mM LiCl (pH = 4), an additional pair of transfer peaks with a mid-point potential at −0.064 V (**peak B**) was observed (Fig. 1 (b)). **Peak B** probably arises from the transfer of a hydrolyzed [AuCl$_4$]$^-$ species, as [AuCl$_4$]$^-$ can undergo stepwise hydrolysis (Eqs. (3) and (4)) forming [AuCl$_3$(OH)]$^-$ and [AuCl$_2$(OH)$_2$]$^-$ at pH = 5 in the presence of 10 mM Cl$^-$ [11] (Fig. S1).

$$[AuCl_4]^- + OH^- \rightleftharpoons [AuCl_3(OH)]^- + Cl^- \tag{3}$$

$$[AuCl_3(OH)]^- + OH^- \rightleftharpoons [AuCl_2(OH)_2]^- + Cl^- \tag{4}$$

In view of this evidence, a previous assignment of the peak to [AuCl$_2$]$^-$ appears less likely [18]. Assuming that **peak B** corresponds to the transfer of [AuCl$_3$(OH)]$^-$, its ion transfer potential can be estimated from $\Delta_{DCE}^{W}G^{\circ}$ of Cl$^-$ (51.1 kJ mol^{-1} [37] or 46.2 kJ mol^{-1} [38]) and OH$^-$ (67.6 kJ mol^{-1} [37] or 63.3 kJ mol^{-1} [39]) as shown in Table 1. The difference between $\Delta_{DCE}^{W}G^{\circ}$ of Cl$^-$ and that of OH$^-$ is thus 16.8 kJ mol^{-1} on average, close to the difference between the ion transfer potentials of **peaks A** and **B** (17.3 kJ mol^{-1}, Fig. 1(a) and (b)). We therefore propose that **peak B** corresponds to the transfer of [AuCl$_3$(OH)]$^-$. The similarity between the difference in $\Delta_{DCE}^{W}G^{\circ}$

Table 2
EXAFS structural parameters for the Au(III) chloride-hydroxide systems shown in Fig. 2.

NaOH (mM)	pH	Au–Cl	Au–OH			$x_{Au(III)}S_0^2$	Au–Au			ΔE (eV)	R-factor
		$N_{Cl,exp}$	$R_{Cl,exp}$ (Å)	$N_{OH,exp}$	$R_{OH,exp}$ (Å)		σ^2_{Au}(Å^2)	$R_{Au,exp}$ (Å)	$x_{Au(0)}S_0^2$		
0[a]	2.40	4	2.27(2)	—	—	0.88(7)	--	—	—	1.3(8)	0.0214
5	5.75	3.2(2)	2.26(6)	0.77(9)	1.93(3)	0.90(5)	—	—	—	1.2(1)	0.0190
10	7.01	2.4(2)	2.26(1)	1.6(2)	1.95(2)	0.87(4)	—	—	—	0.31(3)	0.0291
15	10.25	1.9(3)	2.23(1)	2.0(8)	1.94(2)	0.70(5)	0.0050(8)	2.85(3)	0.081(1)	−4.7(2)	0.0400
50	11.77	1.2(4)	2.14(7)	2.8(4)	1.93(2)	0.47(2)	0.0091	2.85(1)	0.47(2)	−3.4(2)	0.0130

R denotes the bond length. *N* denotes the coordination number. *x* refers to the relative composition of Au(0) and Au(III) species. S_0^2 refers to amplitude reduction factor. ΔE refers to the shift in energy. Debye-Waller factors σ^2 were kept constant for the scattering paths involving Cl$^-$ and OH$^-$ where σ_{Cl}^2 = 0.00211 Å^2 and, σ_O^2 = 0.00202 Å^2. A k-range of 3–12 Å^{-1} and FT- range of 1–4 Å were used, except for the pH = 11.77 sample where window ranges were 3–10 Å^{-1} and 1.25–4 Å. $N_{OH,exp}$ was calculated from 4–$N_{Cl,exp}$. R-factor defines the goodness of fit. The scattering paths used were Au–Cl, Au–Au and Au–O single scattering paths, Au—Cl— —Cl—Au, Au—O— —O—Au and Au—O — —Cl—Au multiple scattering paths where necessary.
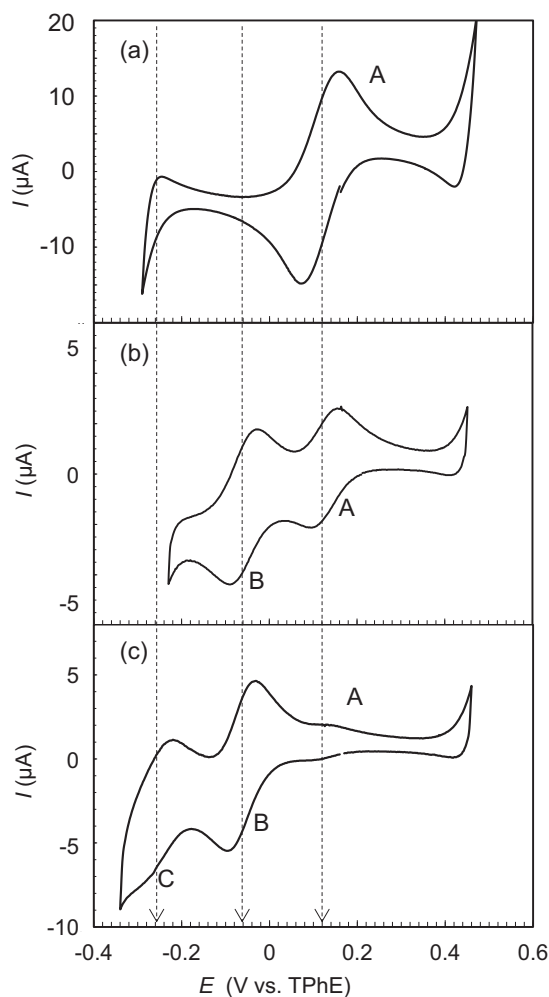
[a] 5 mM HCl.

Fig. 1. The ion transfer voltammogram at a water|DCE interface. The aqueous phases contain either (a) 0.2 mM H⁺[AuCl₄]⁻ and 10 mM HCl; (b) 0.2 mM Na⁺[AuCl₄]⁻ and 10 mM LiCl; or (c) 0.2 mM Na⁺[AuCl₄]⁻ and 5 mM Li₂SO₄. The DCE phase for all samples contain 10 mM TOA⁺TFPB⁻. The linear dashed lines indicate the mid-point potentials. The scan rate was 10 mV s⁻¹.

[Cl⁻—OH⁻], and the difference between ion transfer potentials of **peaks A** and **B** suggests that the latter is dependent on the difference between the solvation energies of Cl⁻ and OH⁻ in water and DCE, rather than the difference between Au—Cl and Au—OH bond strengths.

When 5 mM Li₂SO₄ was used instead of LiCl (Fig. 1(c)), another pair of negative and positive peaks with a mid-point potential at −0.254 V (**peak C**) was observed in addition to **peaks A and B**. SO₄²⁻ is more hydrophilic than Cl⁻ therefore extending the negative region of the potential window [38]. **Peak C** is assigned to the transfer of [AuCl₂(OH)₂]⁻ because the difference of the mid-point potentials of **peaks B** and **C** is close to the difference between the $\Delta_{DCE}^{W} G^{\circ}$ of Cl⁻ and OH⁻, in a similar manner to the assignment of **peak B** to [AuCl₃(OH)]⁻ described above.

The dependence of the Au(III) hydrolysis on H⁺ concentration was investigated at a constant Cl⁻ concentration of 10 mM (Fig. S2). **Peak A** attributed to the transfer of [AuCl₄]⁻ was seen to be more pronounced as H⁺ concentration was increased whereas **peak B** assigned to [AuCl₃(OH)]⁻ was only observed at lower H⁺ concentrations. Based on the data obtained, we suggest that the pre-peak observed in the literature [9] when 10 mM KCl was employed as a supporting electrolyte in water corresponds to the transfer of [AuCl₃(OH)]⁻. In addition, the dependence of Au(III)

hydrolysis on Cl⁻ concentration was independently examined at a constant H⁺ concentration of 10 mM (Fig. S3). In this case p**eak A** corresponding to the transfer of [AuCl₄]⁻ increases with an increase in Cl⁻ concentration. P**eak B** assigned to [AuCl₃(OH)]⁻ was observed at lower concentrations of Cl⁻. When no Cl⁻ was added, both **peaks A** and **B** are less pronounced because of the preferential formation of [AuCl₂(OH)₂]⁻ through further hydrolysis of Au(III) as observed as **peak C** in Fig. 1.

[AuCl₄]⁻ hydrolysis as a function of pH was followed by XAS (Fig. 2). Solution pH was varied by the addition of OH⁻ while maintaining a constant Cl⁻ concentration at 0.5 M. [AuCl₄]⁻ in an acidic solution (pH 2.40) was also measured to serve as a reference. The strong white line at 11 920 eV showed constant intensity, except for the most basic case at 50 mM OH⁻ (pH = 11.77, Fig. 2(a)). The presence of the intense white line for all the solutions indicates that the gold oxidation state remained at +III independent of pH. The FT peak at 1.87 Å (before phase shift, Fig. 2(c)) corresponding to the Au—Cl scattering path, decreased in intensity with increasing pH. As Cl⁻ was gradually exchanged with OH⁻ with an increase in pH, the somewhat shorter FT peak at 1.55 Å became more intense. The weaker intensity of the Au—OH scattering path arises from the fact that oxygen is a lighter element than chlorine, with fewer core electrons and hence a smaller back-scattering amplitude. The coordination numbers of Cl⁻ and OH⁻ ($N_{Cl,exp}$ and $N_{OH,exp}$) and the bond distances of Au—Cl and Au—OH ($R_{Cl,exp}$ and $R_{OH,exp}$) were quantified from the EXAFS data and plotted as a function of pH (Table 2 and Fig. 3). The decrease in $N_{Cl,exp}$ with pH is accompanied by an increase in $N_{OH,exp}$. $R_{Cl,exp}$ decreased with increasing pH, whereas $R_{OH,exp}$ was constant. The average coordination numbers of Cl⁻ and OH⁻ were calculated from the stability constants of Au(III)—Cl—OH complexes ($N_{Cl,cal}$ and $N_{OH,cal}$) [11] at each pH (Fig. 3). It was found that $N_{Cl,exp}$ and $N_{OH,exp}$ at pH 2.40, 5.75, and 7.01 were very close to $N_{Cl,cal}$ and $N_{OH,cal}$. For instance at pH 5.75, a solution composition of 34% [AuCl₄]⁻, 58% [AuCl₃(OH)]⁻ and 8% [AuCl₂(OH)₂]⁻ was predicted; thus $N_{Cl,cal} = 3.32$ and $N_{OH,cal} = 0.68$ which are in very good agreement with $N_{Cl,cal} = 3.2$ (2) and $N_{OH,cal} = 0.77(9)$. However, $N_{Cl,exp}$ and $N_{OH,exp}$ at pH = 10.25 and 11.77 deviated from the $N_{Cl,cal}$ and $N_{OH,cal}$ values expected for homogeneous molecular hydroxo complexes [11] because of metallic Au formation. The EXAFS analysis revealed Au—Au scattering, i.e. the presence of metallic Au. The Au—Au scattering parameters have also been included in Table 2.

3.2. Stability of [AuCl₂]⁻ in water as a function of pH and Cl⁻ concentration

The chemical stability of [AuCl₂]⁻ in water was investigated in the presence of either HCl, LiCl or Li₂SO₄ (Fig. 4). There are few reliable papers on the stability of [AuCl₂]⁻ in aqueous solution because of the spontaneous disproportionation of [AuCl₂]⁻ at ambient conditions [13,30]. Since [AuCl₂]⁻ is stable in DCE [22], voltammetry for the transfer of [AuCl₂]⁻ at the water | DCE interface is used here to shed more light on the stability of this complex. The stability of [AuCl₂]⁻ in acidic aqueous solutions was examined in the same way as that of [AuCl₄]⁻ above.

A voltammogram at the interface between an aqueous solution with 10 mM HCl (pH = 2) and a DCE phase containing 0.2 mM TOA⁺[AuCl₂]⁻ and 10 mM TOA⁺TFPB⁻ was recorded (Fig. 4-a). Positive and negative currents were observed at 0.058 and −0.004 V, which were controlled by the diffusion of [AuCl₂]⁻ from DCE to water. The mid-point potential was 0.026 V (**peak D**). To examine the stability of [AuCl₂]⁻ in acidic aqueous solutions a controlled potential electrolysis experiment was carried out. Under the same reactant conditions as above, a potential of 0.4 V was applied for 30 min as a means to extract AuCl₂⁻ into the aqueous phase electrochemically. The voltammogram measured
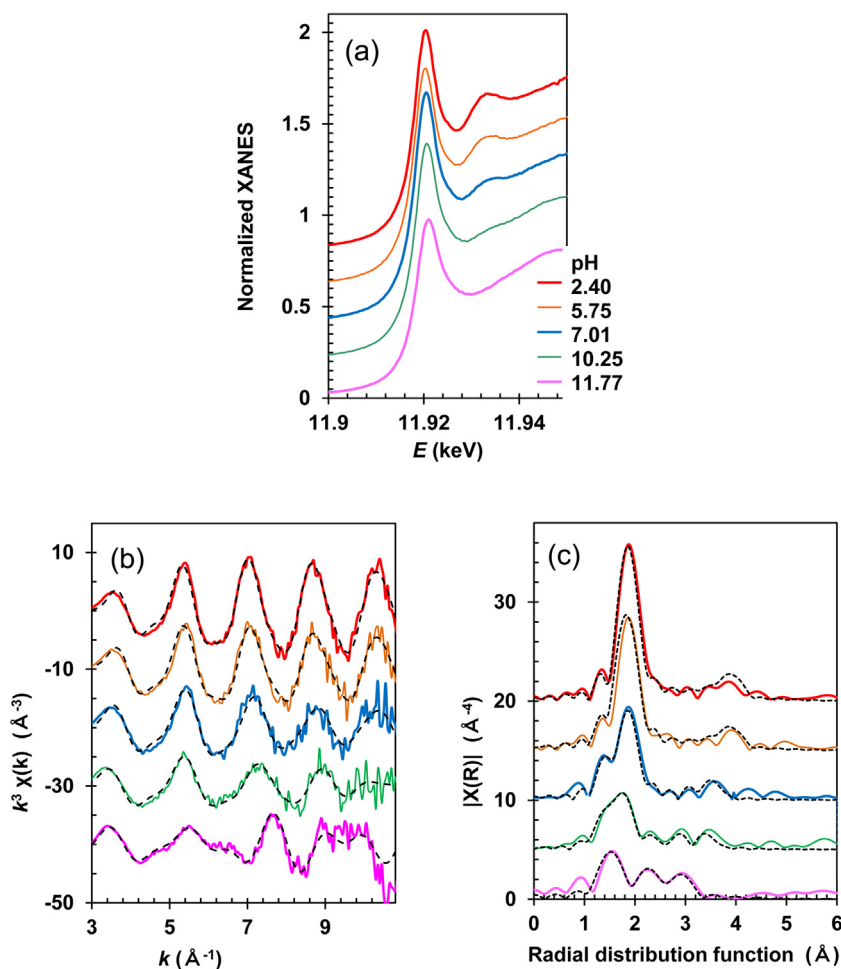
Fig. 2. XAFS of the Au—Cl—OH solution systems as a function of pH. All samples contain 5 mM Na$^+$[AuCl$_4$]$^-$ and 500 mM NaCl. The pH 2.40 sample contains 5 mM HCl. The pH 5.75, 7.01, 10.25 and 11.77 samples contain 5, 10, 15 and 50 mM NaOH respectively. (a) The normalized XANES spectra. (b) The k^3-weighted EXAFS spectra and (c) the corresponding FT-space spectra converted from k-space using a window range of 3.0–11 Å^{-1}. The measured spectra are indicated by solid lines and the fitted spectra by dashed lines.

after the transfer (data not shown) was very similar to the original sample indicating that there was no electrolysis. If [AuCl$_2$]$^-$ was unstable in aqueous solution we would anticipate the development of peaks at the transfer potential of [AuCl$_4$]$^-$ (**peak A**) generated by disproportionation of [AuCl$_2$]$^-$, or a peak at the
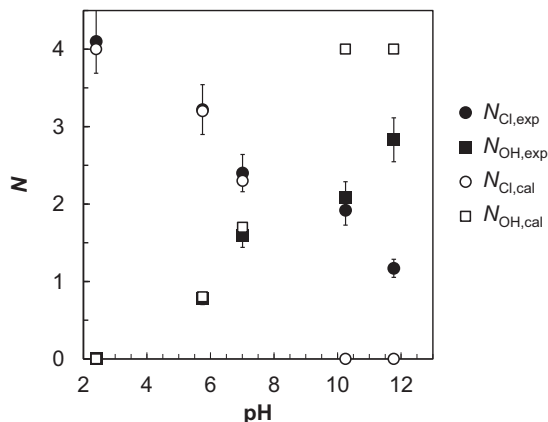

Fig. 3. Dependence of coordination numbers N_{Cl} and N_{OH} on pH. $N_{Cl,exp}$ and $N_{OH,exp}$ are the values determined experimentally using the EXAFS analysis shown in Table 2. $N_{Cl,cal}$ and $N_{OH,cal}$ were calculated based on the stability constants reported in Ref. [11].

negative end of the potential window indicative of hydrolysis of the chloride complex. As no such peaks were visible in Fig. 4(a) we therefore suggest that [AuCl$_2$]$^-$ was stable in the presence of 10 mM HCl.

Surprisingly, 100 mM LiCl produced a very similar response where the diffusion controlled [AuCl$_2$]$^-$ ion transfer was the only peak observed (**peak D**, Fig. 4(b). By analogy with Au(III) hydrolysis, when 100 mM LiCl was used instead of 10 mM HCl, currents corresponding to the transfer of hydrolyzed species such as [AuCl(OH)]$^-$ were expected at the negative end of the potential window. As with HCl, a fixed potential of 0.4 V was applied for 30 min to transfer [AuCl$_2$]$^-$ into the aqueous phase to detect the possible hydrolysis products. However, the initial and final voltammogram was similar suggesting that [AuCl$_2$]$^-$ is stable in a neutral aqueous solution for at least 30 min, possibly because [AuCl$_2$]$^-$ was additionally stabilized by the presence of Cl$^-$ electrolyte.

In line with this, an additional test was carried out to check the stability of [AuCl$_2$]$^-$ in water. An aqueous solution of [AuCl$_2$]$^-$ was prepared by exchange with [AuCl$_4$]$^-$ as described in the experimental section. [AuCl$_2$]$^-$ in water was stable in the short term, but metallic gold was found at the interface after a few hours, indicating the well-known disproportionation of [AuCl$_2$]$^-$ in water to metallic Au and [AuCl$_4$]$^-$ [13], Eq. (5).

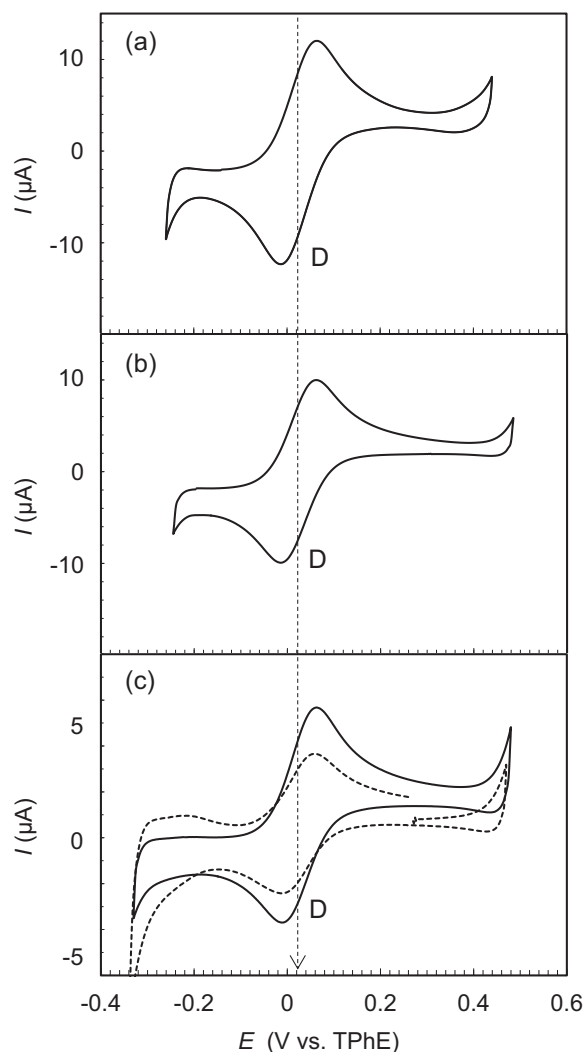$$3[AuCl_2]^- \rightleftharpoons 2Au + [AuCl_4]^- + 2Cl^- \tag{5}$$

Fig. 4. The ion transfer voltammogram at a water|DCE interface. The aqueous phases contain either (a) 10 mM HCl, (b) 100 mM LiCl or (c) 5 mM Li$_2$SO$_4$. The DCE phase for all samples contain 0.2 mM TOA$^+$[AuCl$_2$]$^-$ and 10 mM TOA$^+$TFPB$^-$. Dashed line indicates mid-point potential. The scan rate was 10 mV s^{-1}.

When Li$_2$SO$_4$ was used as the supporting electrolyte therefore lowering the Cl$^-$ and H$^+$ concentrations in the solution, the peak current for the transfer of [AuCl$_2$]$^-$ decreased with each scan. In this case the application of 0.4 V for 1800 s to drive transfer into the aqueous phase did induce electrolysis as shown by the difference in the initial state (solid line) and final state (dotted line) CVs in Fig. 4(c). Also, a broad positive and negative current corresponding to the transfer of Cl$^-$ formed by the disproportionation of [AuCl$_2$]$^-$ was observed at −0.25 V, which is close to the transfer of SO$_4^{2-}$ at −0.32 V (corresponding to the negative end of the potential window).

3.3. Stoichiometric analysis of the reduction of [AuCl$_4$]$^-$ by hexacyanoferrate(II) ion

Ion transfer reactions at the micro-interface between aqueous [AuCl$_4$]$^-$ and hexacyanoferrate(II) and DCE were investigated as a function of the molar ratio of hexacyanoferrate(II) to [AuCl$_4$]$^-$, denoted as **r**. Reduction of [AuCl$_4$]$^-$ and [AuCl$_2$]$^-$ to form metallic Au by the oxidation of hexacyanoferrate(II) would be expected based on the standard potential of [AuCl$_4$]$^-$, [AuCl$_2$]$^-$ and hexacyanoferrate(II) (Table 3). For **r** = 10 where [Fe(CN)$_6$]$^{4-}$ = 5 mM

Table 3
Standard potential of each redox couple in water [43].

Redox couple	ΔE^0 (V vs. NHE)
[AuCl$_4$]$^-$/Au	1.002
[AuCl$_2$]$^-$/Au	1.154
[AuCl$_4$]$^-$/[AuCl$_2$]$^-$	0.93
[Fe(CN)$_6$]$^{3-}$/[Fe(CN)$_6$]$^{4-}$	0.36

and [AuCl$_4$]$^-$ = 0.5 mM, a negative current was observed at −0.036 V (**peak E**) in Fig. 5(a-1). The peak potential is more negative than the [AuCl$_2$]$^-$ ion transfer (**peak D**) in Fig. 4(a). We did not observe the transfer of [AuCl$_2$]$^-$ in the presence of [AuCl$_4$]$^-$ and hexacyanoferrate(II). To check if the species corresponding to the transfer peak (**peak E**) was [Au(CN)$_2$]$^-$, a voltammogram between aqueous K$^+$[Au(CN)$_2$]$^-$ and DCE was measured.

The negative current corresponding to the transfer of [Au(CN)$_2$]$^-$ was indeed observed (Fig. 6). The half wave potential for the transfer of [Au(CN)$_2$]$^-$ agreed with that obtained in **r** = 10 in Fig. 5(a-1). These results indicate the concomitant reduction of Au (III) to Au(I) and ligand exchange. Although [AuCl$_2$]$^-$ was not observed we cannot rule out its possible involvement as a fast lived intermediate as per Eq. (6). The [AuCl$_2$]$^-$ generated in water may then form a complex with hexacyanoferrate(II) or hexacyanoferrate(III) to yield [Au(CN)$_2$]$^-$ as Eqs. (7) and/or (8) [8].

$$[AuCl_4]^- + 2[Fe(CN)_6]^{4-} \rightleftharpoons [AuCl_2]^- + 2[Fe(CN)_6]^{3-} + 2Cl^- \quad (6)$$

$$[AuCl_2]^- + [Fe(CN)_6]^{4-} \rightleftharpoons [Au(CN)_2]^- + [Fe(CN)_4Cl_2]^{4-} \quad (7)$$

And/or

$$[AuCl_2]^- + [Fe(CN)_6]^{3-} \rightleftharpoons [Au(CN)_2]^- + [Fe(CN)_4Cl_2]^{3-} \quad (8)$$
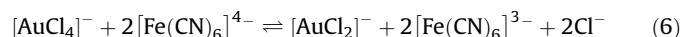
XAS characterization of this system of coupled equilibria was conducted under conditions similar to those of the voltammetric measurements again examining HAuCl$_4$ and hexacyanoferrate(II) solutions at different values of **r**. Fig. 7(a) shows XANES spectra for Au complexes as a function of hexacyanoferrate(II) concentration. The spectra of [AuCl$_4$]$^-$ and [Au(CN)$_2$]$^-$ in the absence of hexacyanoferrate (II) were also measured as references (Fig. 7(a)). Fig. 7(b) and (c) show the k^3-weighted EXAFS spectra and their corresponding Fourier transforms. As expected with increasing **r**, the FT peak at ~1.8 Å (before phase shift, Fig. 7(c)) corresponding to Au—Cl decreased and the ~1.5 and 2.8 Å peaks corresponding to Au—CN became more intense. We performed linear combination fitting at each value of **r** (0.5, 1, 2 and 5) assuming only [Au(CN)$_2$]$^-$ and [AuCl$_4$]$^-$ in the solution (Fig. 8(a) and (b), and Fig. S4). Good fits can be obtained for **r** = 2 and 5 where hexacyanoferrate(II) is in excess resulting in a predominantly [Au(CN)$_2$]$^-$ solution. In contrast, data for **r** = 0.5 and 1 suggest the presence of an unknown intermediate in the region of 11 924 eV where the fits could not be described by a combination of [AuCl$_4$]$^-$ and [Au(CN)$_2$]$^-$. We examined the possible presence of [Au(CN)$_4$]$^-$ or [AuCl$_2$]$^-$ [22] (fits not shown) but neither offered a good fit and principal component analysis did not suggest their presence in the sample. As such further analysis is required to determine the structure of the unknown species. The standards mentioned here are provided for reference in Fig. S5. At **r** = 2 and higher, the Au—CN species is dominant based on both EXAFS observations and XANES linear combination analysis which is in line with the anticipated stoichiometry of the reaction where two moles of hexacyanoferrate(II) are required to reduce one mole of [AuCl$_4$]$^-$.

It can therefore be concluded that [Au(CN)$_2$]$^-$ must be the species responsible for **peak E** in the presence of excess
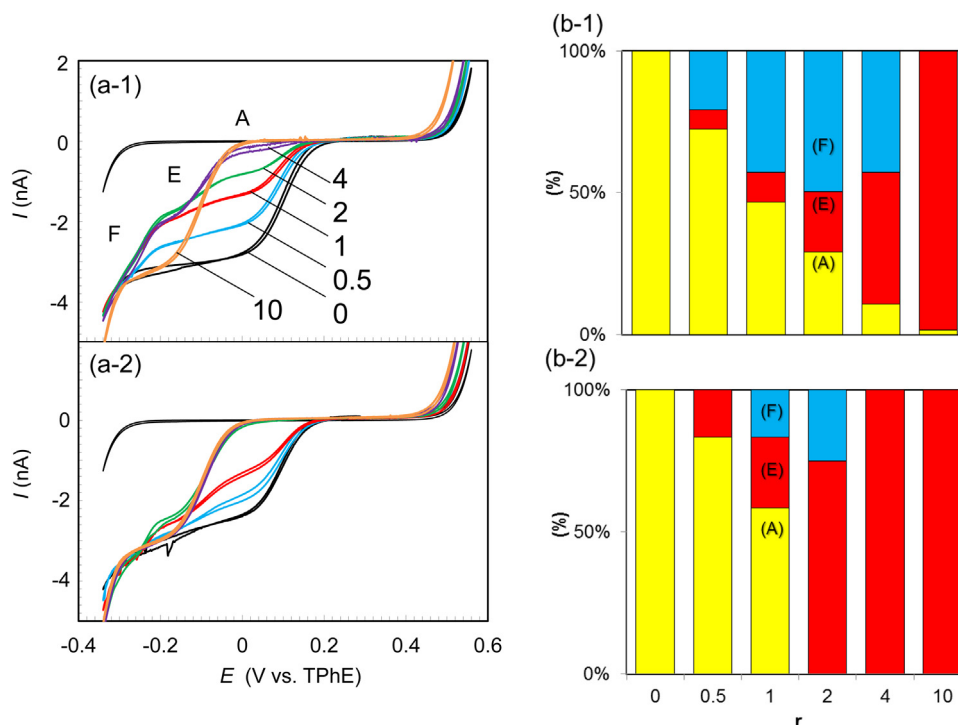
Fig. 5. The reaction between AuCl$_4^-$ and hexacyanoferrate(II) as a function of **r**. The aqueous phases contain 0.5 mM H$^+$[AuCl$_4$]$^-$, 10 mM HCl and either 0, 0.25, 0.5, 1, 2 or 5 mM hexacyanoferrate(II) (**r** = 0, 0.5, 1, 2, 4 or 10). The DCE phase contains 10 mM TOA$^+$TFPB$^-$. (a) The cyclic voltammogram was measured at a micro interface. The samples were measured either directly after contacting both phases (a-1 and b-1) or 24 h after (a-2 and b-2). **Peaks A,E** and **F** were assigned to the transfers of [AuCl$_4$]$^-$, [Au(CN)$_2$]$^-$ and a currently unidentified intermediate species. The relative compositions of the Au species as a function of **r** (b-1 and b-2) were calculated from the limiting current (a-1 and a-2). The scan rate was 5 mV s^{-1}.

hexacyanoferrate(II) relative to [AuCl$_4$]$^-$ (**r** > 5). On the other hand, the current at −0.1 V (**peak E**) has previously been attributed to the one electron reduction of [AuCl$_4$]$^-$ to "[AuCl$_3$]$^-$" [9] or the transfer of [AuCl$_2$]$^-$ [10]. Our stoichiometric analysis also confirms the conclusion of Harish et al. [7] who suggested the formation of [Au(CN)$_2$]$^-$ on the basis of the high stability constant of [Au(CN)$_2$]$^-$ (ca.10^{38}) compared to that of [AuCl$_4$]$^-$ (ca.10^{25}) and that of [AuCl$_2$]$^-$ (ca.10$^{9.7}$) [13].

Alongside the reaction between [AuCl$_4$]$^-$ and hexacyanoferrate (II), hexacyanoferrate(II) could decompose into hexacyanoferrate (III) which would in turn form Prussian blue with hexacyanoferrate (II) according to Eq. (9) [40]. We confirmed the presence of Prussian blue by UV–vis spectroscopy in this study (data not shown). We note that no reaction was observed between aqueous [AuCl$_4$]$^-$ and hexacyanoferrate(III) not hexacyanoferrate(II) described above.

$$K^+ + Fe^{3+} + [Fe(CN)_6]^{4-} \rightleftharpoons K^+ Fe^{3+} [Fe(CN)_6] \qquad (9)$$
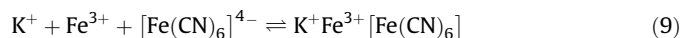
Recall that in the VCTIES experiment described earlier in this section (Figs. 1 and 5(a-1)), the first negative current (**peak A**) was assigned to the transfer of [AuCl$_4$]$^-$ from water to DCE. **Peak A** remains similar even after the sample was aged for one day. The relative compositions of each species can be quantified from the limiting currents obtained in the VCTIES. The cyclic voltammetry for the fresh samples are shown in Fig. 5(a-1) with the relative compositions for the samples shown in Fig. 5(b-1); the samples aged for one day are shown in Fig. 5(a-2) and (b-2). When a two-fold excess of hexacyanoferrate(II) to [AuCl$_4$]$^-$ was added, i.e. **r** = 2, a second negative current (**peak E**) corresponding to the transfer of [Au(CN)$_2$]$^-$ was also observed with 21.3% for the fresh sample and gradually changed to 75.0% after ageing for one day; the trend is expected because [Au(CN)$_2$]$^-$ is the reaction product. Interestingly,

an additional ion transfer peak was observed for **r** = 0.5, 1, 2 and 4 for the fresh samples at −0.25 V (**peak F**), which is close to the negative current limit (transfer of Cl$^-$ as a supporting electrolyte). The limiting current of **peak F** was found to decrease after 1 day. Although initially present in all samples apart from **r** = 0 and **r** = 10 after 24 h, the signal only remained present for **r** = 1 and 2, having decreased from 42.7% to 16.7% for the **r** = 1 sample and from 49.7% to 25.0% for the **r** = 2 sample. Thus, we suggest that **peak F** corresponds to a transient intermediate species in the reaction between [AuCl$_4$]$^-$ and hexacyanoferrate(II).

Cheng et al. [9] reported a peak similar to **peak F**. They assigned the peak to the electron transfer at the interface corresponding to the reduction of [AuCl$_4$]$^-$ to metallic Au in DCE, accompanied by

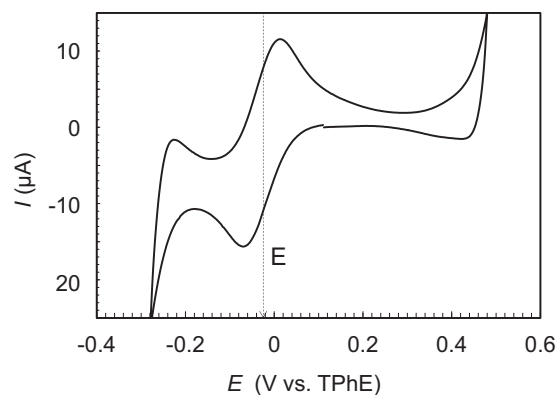**Fig. 6.** The cyclic voltammogram showing the transfer of [Au(CN)$_2$]$^-$. The aqueous phase contains 0.2 mM K$^+$[Au(CN)$_2$]$^-$ and 10 mM HCl. The DCE phase contains 10 mM TOA$^+$TFPB$^-$. The scan rate was 10 mV s^{-1}.
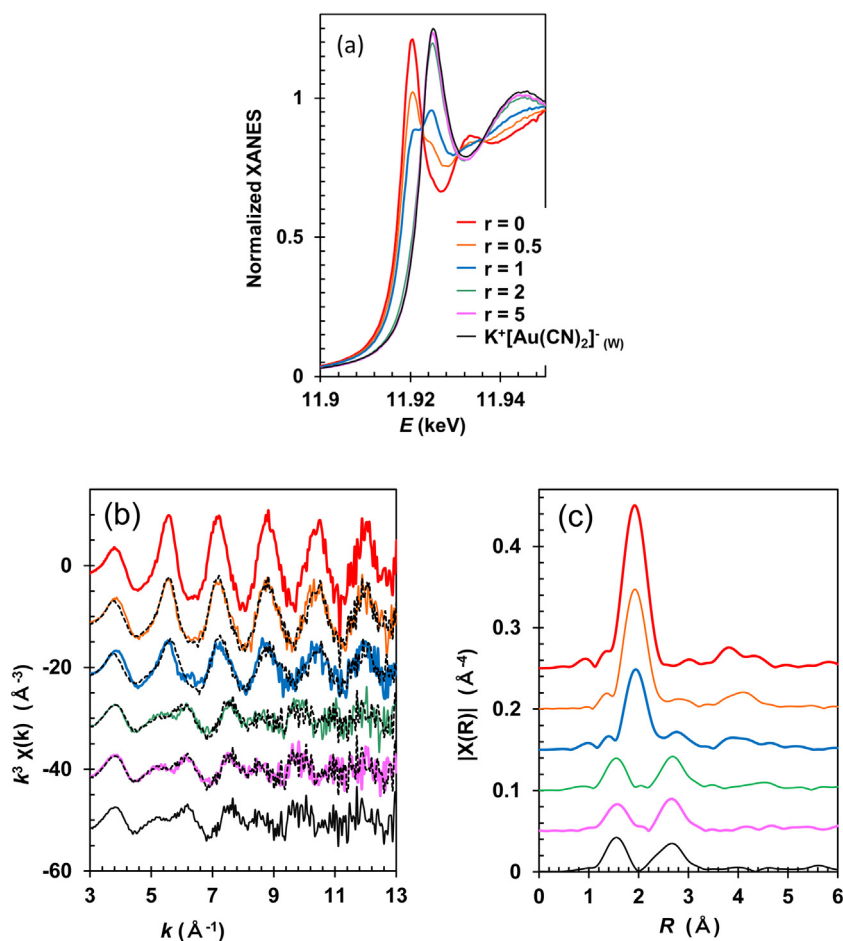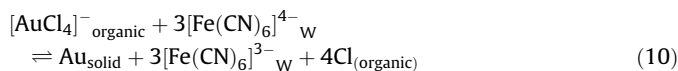
Fig. 7. XAFS spectra of the Au—Cl—CN solution systems. The solutions contain 5 mM H$^+$[AuCl$_4$]$^-$ and either 0, 2.5, 5, 10 or 25 mM hexacyanoferrate(II) (**r** = 0, 0.5, 1, 2 or 5). (a) The XANES spectra. (b) The k^3-weighted EXAFS spectra and (c) the corresponding FT-space spectra.

the oxidation of hexacyanoferrate(II) to hexacyanoferrate(III) as per Eq (10).

$$[AuCl_4]^-_{organic} + 3[Fe(CN)_6]^{4-}_W$$
$$\rightleftharpoons Au_{solid} + 3[Fe(CN)_6]^{3-}_W + 4Cl_{(organic)} \qquad (10)$$

If the electron transfer reaction described in Eq. (10) were to occur, Cl$^-$ would form in the organic solution instead of the aqueous. However, no current for the transfer of Cl$^-$ from the organic to the aqueous phase was observed within the potential window of the voltammogram (Fig. 5(a)).

3.4. Stoichiometric analysis of the reduction of [AuCl$_2$]$^-$

To further investigate the identity of the unknown **peak F** we examined the possibility of reactions between hexacyanoferrate (II) and [AuCl$_2$]$^-$. Even though the presence of [AuCl$_2$]$^-$ was not detected by VCTIES or XAFS, considering that (i) [Au(CN)$_2$]$^-$ is formed, and that (ii) [AuCl$_2$]$^-$ is itself able to react with hexacyanoferrate (II), [AuCl$_2$]$^-$ could possibly be an intermediate for the reaction between [AuCl$_4$]$^-$ and hexacyanoferrate (II). Fig. 9(a) shows the voltammogram recorded at the macro interface between an aqueous phase containing hexacyanoferrate(II) and a DCE phase containing TOA$^+$[AuCl$_2$]$^-$. Here, [AuCl$_2$]$^-$ was directly dissolved in DCE to speed up the reaction with hexacyanoferrate (II). In the first scan, a positive current for the transfer of [AuCl$_2$]$^-$ from DCE to water was observed (**peak D**). The negative current pair for the return transfer of [AuCl$_2$]$^-$ from water to DCE was however not observed as the [AuCl$_2$]$^-$ was consumed by the

reaction. Instead, when the potential cycle was repeated, the positive current seemingly shifted to a more negative potential (from 0.045 V to 0.005 V) because of the formation of [Au (CN)$_2$]$^-$ through ligand exchange between [AuCl$_2$]$^-$ and hexacyanoferrate (II) in the aqueous phase as per Eq. (7).

This was then compared to a voltammogram for the presence of hexacyanoferrate(III) instead of hexacyanoferrate(II) and DCE containing [AuCl$_2$]$^-$ is shown in Fig. 9(b). Hexacyanoferrate(III) had failed to react with [AuCl$_4$]$^-$. The positive current for the transfer of [AuCl$_2$]$^-$ from DCE to water (**peak D**) decreased with successive scans and the corresponding negative current was not observed. However, positive and negative currents at −0.2 V were observed. Even though the ion transfer current of [AuCl$_2$]$^-$ decreased with scan number, the transfer of [Au(CN)$_2$]$^-$ which could be formed by the ligand exchange reaction with [AuCl$_2$]$^-$ and hexacyanoferrate(III) was not observed. Therefore, assuming that the reactions proceed via the substitution pathway shown above, the mechanism was via Eq. (7) and not Eq. (8), during the experiment. These results indicate that the positive and negative currents at −0.2 V correspond to an ion transfer reaction (instead of an electron transfer reaction) between water and DCE as there is no redox reaction in this example, and that the ionic species formed is more hydrophilic than [AuCl$_2$]$^-$ and [Au(CN)$_2$]$^-$ based on the ion transfer potentials.

To confirm that the formation of the unknown species is occurring in the aqueous phase, an aqueous [AuCl$_2$]$^-$ solution was prepared. Even though ion transfer of [AuCl$_2$]$^-$ was observed in the absence of hexacyanoferrate(III) (dotted line in Fig. 10), a negative

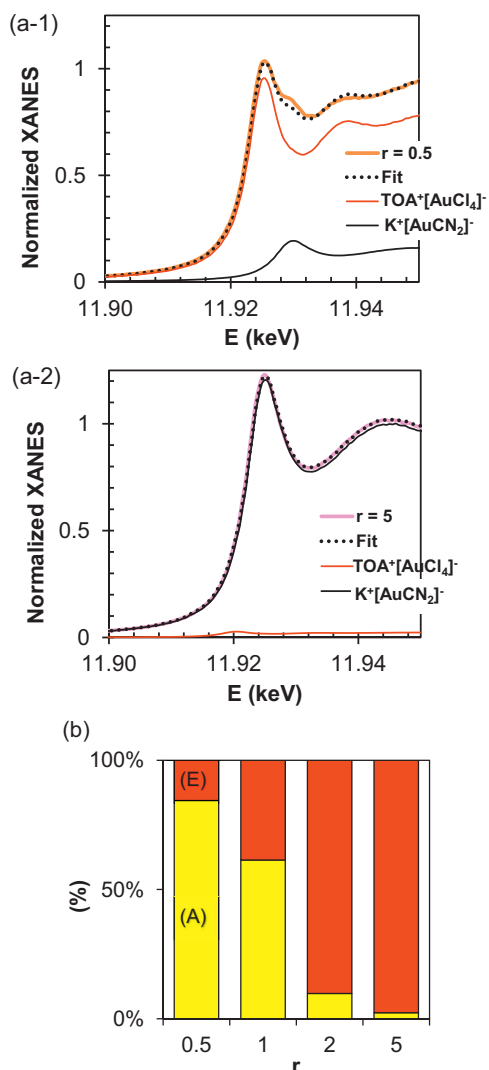Fig. 8. Linear combination fitting of XANES spectra collected in a single aqueous phase solution at different **r**. The solution contains 5 mM H$^+$[AuCl$_4$]$^-$ and either 2.5 mM hexacyanoferrate(II) (**r** = 0.5, a-1) or 25 mM hexacyanoferrate(II) (**r** = 5, a-2). For both (a-1) and (a-2) the original spectra are plotted alongside the linear combination fitting result (dotted line) and the relative ratios of the fitting components AuCl$_4^-$ and AuCN$_2^-$. (c) The relative ratios of the fitting components AuCl$_4^-$ and AuCN$_2^-$ as a function of **r**.

and positive current at −0.2 V was observed in the presence of hexacyanoferrate(III) (solid line in Fig. 10), verifying that the unknown ionic species is formed.

3.5. Interfacial nanoparticle synthesis

We have been able to make observations with regard to the stability of Au species in solution. The voltammetry data suggests that the hydrolysis of Au species is dependent on the Cl$^-$ ion concentration as well as the strong influence of pH. A high pH or low Cl$^-$ concentration results in the formation of Au hydrolysis products ([AuCl$_3$(OH)]$^-$ or [AuCl$_2$(OH)$_2$]$^-$). A mixture of Au species has a significant influence on nanoparticle formation because of the different reduction potentials of the Au complexes. For instance, the hydrolysis species of Au(III) halides as well as cyanide species of Au(III) and Au(I) do not easily react with reducing agents. Mixed speciation can therefore result in size polydispersity or a reduction in the concentration of nanoparticles formed [41].
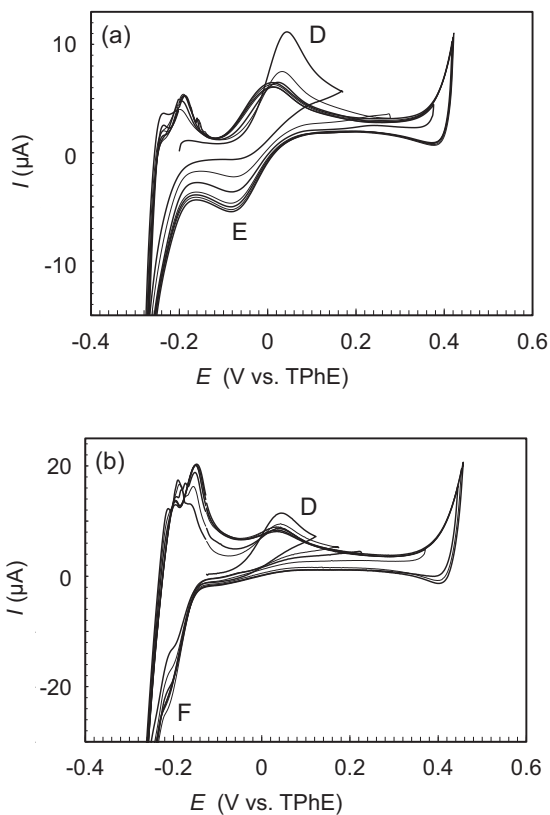

Fig. 9. Cyclic voltammogram at a water|DCE interface. The aqueous phase contains 10 mM HCl and either 5 mM (a) hexacyanoferrate(II) or (b) hexacyanoferrate(III). In both cases, the organic phase contained 0.2 mM TOA$^+$[AuCl$_2$]$^-$ and 10 mM TOA$^+$TFPB$^-$. The scan rate was 10 mV s^{-1}.

Examination of the reduction of [AuCl$_4$]$^-$ by hexacyanoferrate (II) was motivated by the previous by the work of Cheng and Schiffrin on the interfacial reduction of organic TOA$^+$[AuCl$_4$]$^-$ by hexacyanoferrate(II) [9]. In their report electron transfer at the liquid/liquid interface results in the formation of gold nanoparticles which are stabilized at the interface. However our own observations for the system in aqueous solution have instead pointed to the preferential formation of [Au(CN)$_2$]$^-$ which appears to be too stable to undergo further reduction by hexacyanoferrate (II). Previous reports have indicated that nanoparticles can be
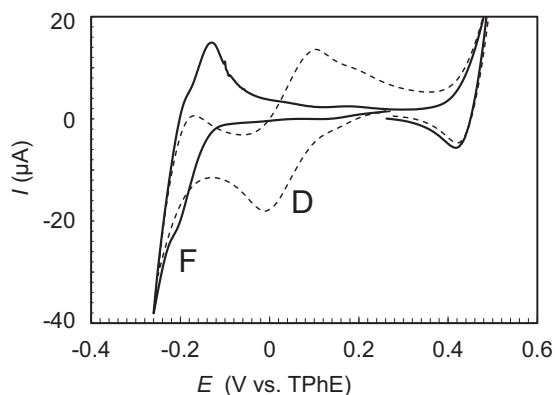

Fig. 10. Cyclic voltammogram at a water|DCE interface. The aqueous phase contains 0.5 mM [AuCl$_2$]$^-$ and 10 mM HCl either in the absence (dotted line) or presence (solid line) of 2.5 mM hexacyanoferrate(II). The DCE phase contains 10 mM TOA$^+$TFPB$^-$. The scan rate was 10 mV s^{-1}. Voltammetric measurements were carried out directly after the preparation of aqueous phase [AuCl$_2$]$^-$ through ion exchange with [AuCl$_4$]$^-$ as described in section 2.1.

formed by the reduction of $[Au(CN)_2]^-$ by the stronger reducing agent sodium borohydride [42].

4. Conclusions

The chemical stability of $[AuCl_4]^-$ and $[AuCl_2]^-$ have been investigated as a function of electrolyte concentration and pH. Using VCTIES, $[AuCl_4]^-$ was found to undergo hydrolysis at high pH and low Cl^- concentration as has been shown in previous studies. In the case of measurements at the liquid/liquid interface it has been shown that the difference between $\Delta_{DCE}^W G°$ of $[AuCl_4]^-$ and $[AuCl_3(OH)]^-$ was close to the difference between $\Delta_{DCE}^W G°$ of Cl^- and OH^-. The XAFS data shows a clear pH dependence on Au hydrolysis which agrees well with calculations based on stability constants in acidic conditions, however at high pH the data suggests that there is a higher concentration of chlorinated Au(III) species than would be anticipated by stability constants possibly due to the formation of metallic Au species. The $N_{Cl,exp}$ and $N_{OH,exp}$ at neutral pH calculated using the EXAFS agreed with $N_{Cl,cal}$ and $N_{OH,cal}$ calculated from the stability constants of Au–Cl–OH complexes. The decomposition of $[AuCl_2]^-$ in aqueous phase was observed at neutral pH and in the absence of Cl^-.

Using the combination of VCTIES and XAFS experiments we have been able to examine the reaction between $[AuCl_4]^-$ and hexacyanoferrate(II) in water. It was found that $[AuCl_4]^-$ readily underwent reduction by hexacyanoferrate(II) to form $[Au(CN)_2]^-$. The formation of $[Au(CN_2)]^-$ was confirmed through calculations of the $\Delta_{DCE}^W G°$ and XAFS linear combination analysis. The reaction is complicated by the presence of an as yet undetermined intermediate species which was consumed within 24 h at most values of **r** investigated, however it was stable enough to be measured by both VCTIES and XAFS. The species is shown by VCTIES to be more hydrophilic than $[Au(CN)_2]^-$, $[AuCl_2]^-$ and $[AuCl_4]^-$. Although not directly detected by VCTIES or XAFS, $[AuCl_2]^-$ could be a reaction intermediate as it readily reacts with hexacyanoferrate(II) forming $[Au(CN)_2]^-$ and a peak in the voltammogram that resembles that of the undetermined intermediate species in the reaction of hexacyanoferrate(II) with $[AuCl_4]^-$ (**peak F**). The lack of metallic Au formation by hexacyanoferrate(II) is related to the rapid formation of $[Au(CN)_2]^-$ and the stability of $[Au(CN)_2]^-$ with respect to further reduction.

Acknowledgements

Appendix A. Supplementary data

Supplementary data associated with this article can be found, in the online version, at http://dx.doi.org/10.1016/j.electacta.2015.12.108.

References

[1] M. Brust, M. Walker, D. Bethell, D.J. Schiffrin, R. Whyman, J. Chem. Soc., Chem. Commun. (1994) 801.
[2] P.J.G. Goulet, R.B. Lennox, J. Am. Chem. Soc. 132 (2010) 9582–9584.
[3] Y. Li, O. Zaluzhna, Y.Y.J. Tong, Langmuir 27 (2011) 7366–7370.
[4] S. Wang, K. Qian, X.Z. Bi, W.X. Huang, J. Phys. Chem. C 113 (2009) 6505–6510.
[5] R.P. Allen, J. Bard, Joseph Jordan, CRC Press, 1985.
[6] J.F. Zhai, Y.M. Zhai, S.J. Dong, Colloid Surface A 335 (2009) 207–210.
[7] S. Harish, J. Joseph, K.L.N. Phani, Electrochim Acta 56 (2011) 5717–5721.
[8] O.N. Vrublevskaya, T.N. Vorobyova, H.K. Lee, S.B. Koo, T I Met Finish 85 (2007) 254–259.
[9] Y. Cheng, D.J. Schiffrin, J. Chem. Soc., Faraday Trans. 92 (1996) 3865–3871.
[10] Y. Gründer, H.L.T. Ho, J.F.W. Mosselmans, S.L.M. Schroeder, R.A.W. Dryfe, Phys. Chem. Chem. Phys. 13 (2011) 15681.
[11] A. Usher, D.C. McPhail, J. Brugger, Geochim. Cosmochim. Acta 73 (2009) 3359–3380.
[12] I.V. Mironov, E.V. Makotchenko, J. Solution Chem. 38 (2009) 725–737.
[13] G. Senanayake, Miner. Eng. 17 (2004) 785–801.
[14] K. Lepkova, J. Clohessy, V.J. Cunnane, J. Phys-Condens Mat. 19 (2007) .
[15] C. Johans, R. Lahtinen, K. Kontturi, D.J. Schiffrin, J. Electroanal. Chem. 488 (2000) 99–109.
[16] K. Lepkova, J. Clohessy, V.J. Cunnane, Electrochim. Acta 53 (2008) 6273–6277.
[17] B. Sefer, R. Gulaboski, V. Mirceski, J. Solid State Electrochem. 16 (2012) 2373–2381.
[18] Y. Grunder, J.F.W. Mosselmans, S.L.M. Schroeder, R.A.W. Dryfe, J. Phys. Chem. C 117 (2013) 5765–5773.
[19] A. Uehara, T. Hashimoto, R.A.W. Dryfe, Electrochim. Acta 118 (2014) 26–32.
[20] S.G. Booth, A. Uehara, S.Y. Chang, J.F.W. Mosselmans, S.L.M. Schroeder, R.A.W. Dryfe, J. Phys. Chem. C 119 (2015) 16785–16792.
[21] H.H. Girault, Electroanal Chem 23 (2010) 1–104.
[22] S.Y. Chang, A. Uehara, S.G. Booth, K. Ignatyev, J.F.W. Mosselmans, R.A.W. Dryfe, S.L.M. Schroeder, Rsc Advances 5 (2015) 6912–6918.
[23] F. Farges, J.A. Sharps, G.E. Brown, Geochim. Cosmochim. Acta 57 (1993) 1243–1252.
[24] X. Chen, W.S. Chu, D.L. Chen, Z.H. Wu, A. Marcelli, Z.Y. Wu, Chem. Geol. 268 (2009) 74–80.
[25] K. Paclawski, D.A. Zajac, M. Borowiec, K. Kapusta, K. Fitzner, J. Phys. Chem. A 114 (2010) 11943–11947.
[26] J. Gaudet, K.K. Bando, Z. Song, T. Fujitani, W. Zhang, D.S. Su, S.T. Oyama, J. Catal. 280 (2011) 40–49.
[27] P.S.G. Kim, Y.F. Hu, Y.M. Yiu, T.K. Sham, J. Electron. Spectrosc. 144 (2005) 811–815.
[28] Z. Song, J.P.L. Kenney, J.B. Fein, B.A. Bunker, Geochim. Cosmochim. Acta 86 (2012) 103–117.
[29] J. Ohyama, K. Teramura, Y. Higuchi, T. Shishido, Y. Hitomi, K. Kato, H. Tanida, T. Uruga, T. Tanaka, Chemphyschem 12 (2011) 127–131.
[30] G.S. Pokrovski, B.R. Tagirov, J. Schott, E.F. Bazarkina, J.L. Hazermann, O. Proux, Chem. Geol. 259 (2009) 17–29.
[31] G. Taylor, H.H.J. Girault, J. Electroanal. Chem. 208 (1986) 179–183.
[32] M.C. Osborne, Y. Shao, C.M. Pereira, H.H. Girault, J. Electroanal. Chem. 364 (1994) 155–161.
[33] H. Ohde, A. Uehara, Y. Yoshida, K. Maeda, S. Kihara, J. Electroanal. Chem. 496 (2001) 110–117.
[34] A.J. Parker, Chem. Rev 69 (1969) 1.
[35] J.F.W. Mosselmans, P.D. Quinn, A.J. Dent, S.A. Cavill, S.D. Moreno, A. Peach, P.J. Leicester, S.J. Keylock, S.R. Gregory, K.D. Atkinson, J.R. Rosell, J. Synchrotron Radiat 16 (2009) 818–824.
[36] B. Ravel, M. Newville, J. Synchrotron Radiat 12 (2005) 537–541.
[37] A.J. Olaya, M.A. Méndez, F. Cortes-Salazar, H.H. Girault, J. Electroanal. Chem. 644 (2010) 60–66.
[38] M. Zhou, S.Y. Gan, L.J. Zhong, X.D. Dong, J. Ulstrup, D.X. Han, L. Niu, Phys. Chem. Chem. Phys. 14 (2012) 3659–3668.
[39] M. Zhou, S.Y. Gan, L.J. Zhong, B. Su, L. Niu, Anal. Chem. 82 (2010) 7857–7860.
[40] R.J. Mortimer, D.R. Rosseinsky, J. Chem. Soc. Dalton Trans. (1984) 2059–2061.
[41] A. Uehara, S.G. Booth, S.Y. Chang, S.L.M. Schroeder, T. Imai, T. Hashimoto, J.F.W. Mosselmans, R.A.W. Dryfe, J. Am. Chem. Soc 137 (2015) 15135–15144.
[42] C.C. Huang, W.C. Lai, C.Y. Tsai, C.H. Yang, C.S. Yeh, Chem. -Eur. J. 18 (2012) 4107–4114.
[43] L.W.J. Heusler, K.E, Standard Potentials in Aqueous Solution, in: A.J. Bard, R. Parsons, J. Jordan (Eds.), Marcel Dekker, New York, 1985, pp. 391–412.